PERGAMON

Journal of Structural Geology 24 (2002) 1195–1214

JOURNAL OF STRUCTURAL GEOLOGY

www.elsevier.com/locate/jstrugeo

Structural and metamorphic constraints on ca. 70 Ma deformation of the northern Valhalla complex, British Columbia: implications for the tectonic evolution of the southern Omineca belt

Peter M. Schaubs[a,*], Sharon D. Carr[a], Robert G. Berman[b]

[a]*Ottawa-Carleton Geoscience Centre, Department of Earth Sciences, Carleton University, Ottawa, Ontario, Canada K1S 5B6*
[b]*Geological Survey of Canada, 601 Booth Street, Ottawa, Ontario, Canada K1A 0E8*

Received 1 January 2001; revised 28 March 2001; accepted 16 May 2001

Abstract

Penetrative deformation occurred ca. 70 Ma ago throughout the northern Valhalla complex in Valhalla and Passmore domes and in the Gwillim Creek shear zone, exposed at the deepest structural levels in both domes. Intense strain (S_T) in the Gwillim Creek shear zone (domain II) was synchronous with and outlasted deformation (D_2) throughout the northern complex (domain I). Upper-amphibolite facies peak mineral assemblages define the predominant foliation. Temperature and pressure results, determined from microdomains with established relationships to reaction textures and microstructures, provide constraints on conditions under which deformation occurred. Deformation was synchronous with and outlasted peak metamorphic conditions at all structural levels. Peak conditions of 825°C and 730 MPa and 850°C and 840 MPa were determined for domains I and II, respectively. This was followed by cooling and retrograde garnet breakdown at conditions of 715°C and 490 MPa and 765°C and 730 MPa in domains I and II, respectively. The faster cooling rate per kilometer of exhumation for domain II relative to domain I is consistent with a model of conductive cooling via thrusting of domain II on to a cold footwall. Metamorphism is interpreted to have resulted from crustal thickening and burial to depths of ca. 25 km based on an inferred clockwise P–T path and the paucity of Late Cretaceous intrusions. Lack of retrograde metamorphism throughout the complex and the high degree of annealing of microstructures indicates that the rocks remained above greenschist-facies conditions until they were exhumed in the Early Tertiary on the Valkyr–Slocan Lake extensional shear zone system.

Previous workers have determined that the peak of metamorphism occurred at 72–67 Ma in a restricted locality in the core of Passmore dome, near Vallican. Our study links this dated metamorphism with the structural evolution and metamorphic history throughout the area, and shows that supracrustal rocks at all structural levels in Valhalla and Passmore domes underwent the same metamorphic and deformation event as those near Vallican. Therefore, we assign a ca. 70 Ma age to the penetrative, high-temperature deformation in northern Valhalla complex and the Gwillim Creek shear zone. This coincides with a major period of shortening in the Rocky Mountains of the Foreland belt. Strain in northern Valhalla complex may represent a local transient shear zone that accommodated crustal thickening in the hinterland during orogen-scale compression, or it may be an exhumed part of the basal detachment of the Rocky Mountains.

Keywords: Tectonic evolution; Deformation; Foliation; Geothermobarometry; Exhumation; Omineca Belt; Gwillim Creek shear zones; Reaction textures; Microstructures

1. Introduction

The Omineca belt (Fig. 1), the polydeformed metamorphic and plutonic hinterland of the eastern Canadian Cordillera, underwent orogenesis during Mesozoic to Paleocene crustal shortening and thickening in response to westward underthrusting of the North American craton. Parrish (1995) pointed out the diachronous nature of deformation within the Omineca belt in southern British Columbia, with an apparent pattern of downward younging with structural depth, from ca. 170 Ma at high structural levels in the Selkirk and Cariboo mountains to ca. 55 Ma in the Monashee Mountains. Recent structural and U–Pb geochronological studies support this general pattern (Gibson et al., 1999; Crowley et al., 2001) but also reveal complexities of metamorphic overprinting (Digel et al., 1998; Crowley et al., 2000), a period of Early Cretaceous exhumation in the northern Monashee Mountains (Scammell, 1993), and how foliations may be reactivated during two or more deformation events over a 120 Ma time

* Corresponding author. Now at: CSIRO Exploration and Mining, Australian Resources Research Centre, P.O. Box 1130, Bentley, WA 6102, Australia. Fax: +61-8-6436-8555.
E-mail address: peter.schaubs@csiro.au (P.M. Schaubs).

0191-8141/02/$ - see front matter
PII: S0191-8141(01)00101-8

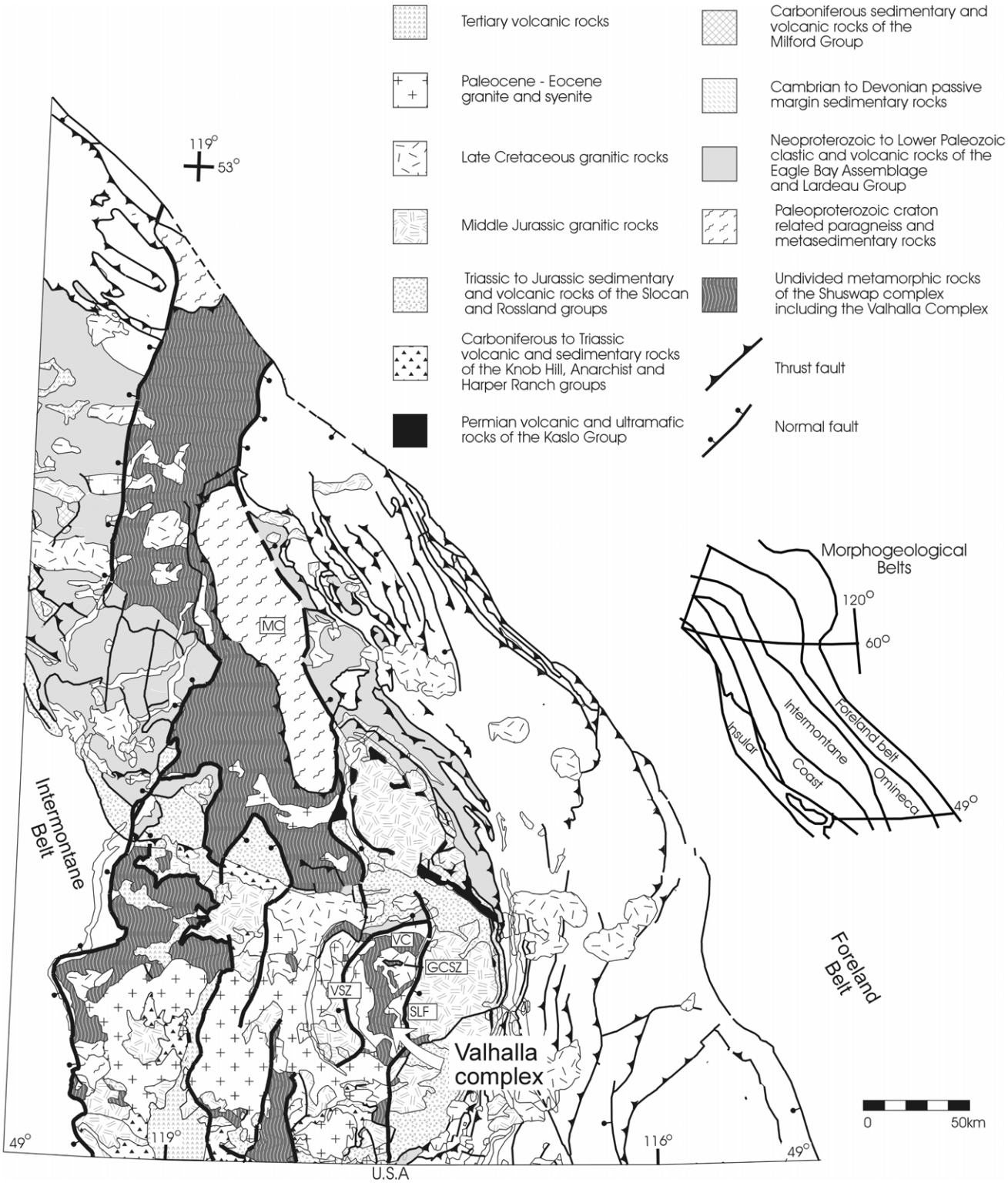

Fig. 1. Tectonic assemblage map of the southern Omineca Belt simplified from Wheeler et al. (1991) and modified after Carr (1991) and Johnson (1994). Note the north–south trending extensional faults superimposed on northwest trending compressional structures. Important tectonic elements include the Monashee complex (MC) and the Valhalla complex (VC), both of which are included in the larger Shuswap complex. Structures in the Valhalla complex include the Gwillim Creek shear zones (GCSZ), Slocan Lake fault (SLF), and the Valkyr shear zone (VSZ).

span (Carr and Simony, 2000a). Foreland belt palinspastic reconstructions require ~150–200 km of Late Cretaceous–Paleocene shortening that must sensibly be transferred across or under the Omineca belt to the plate margin (Price and Mountjoy, 1970; Price, 2000). Williams (1999) pointed out that application of tectonic models for the Omineca belt in the style of the Foreland belt, such as those adopted by Lithoprobe interpretations (Carr, 1995, and references therein; Cook et al., 1992; Brown et al., 1992), are inappropriate. Translation of thrust sheets on ductile shear zones is inconsistent with the structural style of mid-crustal rocks that have flowed in a ductile manner, and neglect the potential significance of ductile thinning during deformation. Rather, Williams (1999) and Brown (2001) propose models whereby transient deformation in the hinterland may change the geometry of the orogenic taper thus indirectly causing thrusting in the Foreland belt. In the light of these ideas, it is clear that we need to characterize the style and timing of deformation and metamorphism throughout the entire structural section in order to refine tectonic models for the Omineca belt, and to propose and test dynamic and geometric models that link the Omineca belt with the Foreland belt to the east.

The results of this study constrain the P–T conditions and timing of deformation throughout a 3-km-thick structural section in the northern Valhalla complex, and contribute to the debate about hinterland tectonic evolution. Two spectacular Cretaceous ductile shear zones are exposed in the core of Valhalla dome in the northern Valhalla complex (Parrish et al., 1987). Very high strain is localized over >0.5-km-thick zones at the lower interface between sheets of ca. 110 Ma granodiorite gneiss and underlying high-grade migmatitic metasedimentary rocks. Rocks that intervene between the shear zones have been interpreted as horses in a ductile thrust system. The two shear-zone strands are interpreted to merge and project into a zone of very strong reflectors imaged in subsurface Lithoprobe seismic reflection data at the latitude of Passmore dome. The Gwillim Creek shear zone has been interpreted to be part of the Late Cretaceous thrust system that accommodated shortening in the Foreland belt (Parrish et al., 1987; Cook et al., 1988; Varsek and Cook, 1994; Carr, 1995; Cook and van der Velden, 1995; Parrish, 1995; Simony and Carr, 2000).

This paper forms part of a study which characterized the lithologic, metamorphic and structural history of supracrustal rocks throughout the northern Valhalla complex in Valhalla and Passmore domes, including the Gwillim Creek shear zone (see also Schaubs 1995; Schaubs and Carr, 1998). The area was studied from a metamorphic and structural perspective, to characterize the relationships between metamorphic reactions and structures in order to place P–T constraints on deformation, and to compare and contrast rocks in the shear zone with less strained rocks throughout the complex. Exposures of the Gwillim Creek shear zone were found along a 100-km-long strike length throughout the entire Valhalla complex. The shear zone projects southward from Valhalla dome to exposures in the core of Passmore dome (Schaubs and Carr, 1998) and the core of the southern Valhalla complex south of Castlegar (Simony and Carr, 1997; Carr and Simony, 2000b). Our results show that near-peak metamorphism at ca. 820–850°C and 720–840 MPa, retrograde decompression to 715°C and 490 MPa (highest structural domain) and 765°C and 720 MPa (lower structural domain), and progressive penetrative deformation throughout the 3 km thick northern Valhalla complex, culminated at ca. 70 Ma, making it the most extensive zone of Late Cretaceous strain documented in the southern Omineca belt. Deformation in the Valhalla complex was concurrent with a major period of shortening in the Foreland belt and may represent a local transient shear zone that accommodated crustal thickening in the hinterland during orogen-scale shortening, or it may be an exhumed part of the basal detachment of the Rocky Mountains.

2. Geology of the Valhalla complex

2.1. Lithology and geometry

The Shuswap complex of the southern Omineca belt comprises mainly sillimanite–K-feldspar-grade rocks which were deformed and metamorphosed in the middle crust during Mesozoic–Paleocene orogenesis and were, in part, exhumed in the lower plate of Early Tertiary extensional fault systems (Fig. 1). The Valhalla complex is a 20×80 km structural culmination situated in the southern part of the larger Shuswap complex (Figs. 1 and 2). The Valhalla complex, including Valhalla and Passmore domes, was first recognized and mapped by Little (1960) and Reesor (1965). It was interpreted by Reesor as a mantled gneiss dome, but has been reinterpreted as an extensional fault-bounded Paleocene to Eocene Cordilleran metamorphic core complex (Carr et al., 1987; Parrish et al., 1988) and extended to the south by Simony and Carr (1997) to include gneisses south of the Columbia River. The Valhalla complex consists of sheets of highly strained migmatitic amphibolite-facies supracrustal rocks interlayered with orthogneiss and variably deformed Paleocene–Eocene granitic rocks (Fig. 2). These sheets are all gently dipping and are disposed in three domal culminations aligned along a north–south axis: the northern Valhalla dome, the central Passmore dome and the southern Valhalla complex (Figs. 3 and 4). For the purposes of this paper we refer to Valhalla and Passmore domes as the northern Valhalla complex to distinguish them from rocks south of the Columbia River, termed the southern Valhalla complex. The Valhalla complex comprises the lower plate of a regional 59–55 Ma ductile-brittle extensional fault system. The ductile extensional Valkyr shear zone bounds the northern, western and southern margins of the complex and is arched over the complex. It is coincident with the

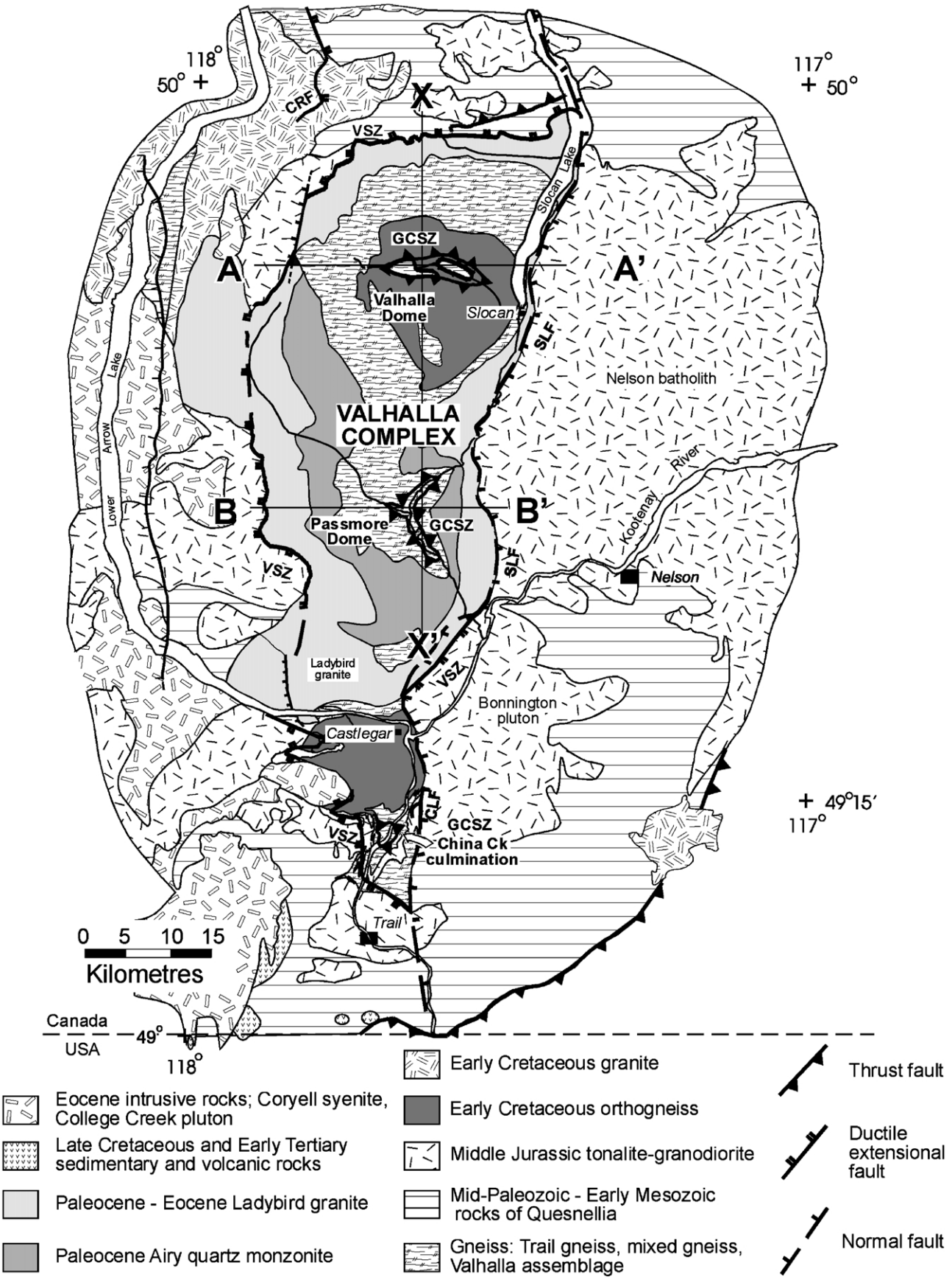
118°
50° +
117°
+ 50°
CRF
VSZ
X
X'
Slocan Lake
GCSZ
A
A'
Valhalla Dome
Slocan
SLF
Nelson batholith
VALHALLA COMPLEX
Arrow Lake
Lower
River
Kootenay
B
B'
Passmore Dome
GCSZ
VSZ
SLF
Nelson
Ladybird granite
VSZ
Bonnington pluton
Castlegar
+ 49°15′
117°
SLF
GCSZ
China Ck culmination
VSZ
Trail
0 5 10 15
Kilometres
Canada
USA
49°
118°
Eocene intrusive rocks; Coryell syenite, College Creek pluton
Late Cretaceous and Early Tertiary sedimentary and volcanic rocks
Paleocene - Eocene Ladybird granite
Paleocene Airy quartz monzonite
Early Cretaceous granite
Early Cretaceous orthogneiss
Middle Jurassic tonalite-granodiorite
Mid-Paleozoic - Early Mesozoic rocks of Quesnellia
Gneiss: Trail gneiss, mixed gneiss, Valhalla assemblage
Thrust fault
Ductile extensional fault
Normal fault

upper margin of sheets of peraluminous leucogranite and pegmatite of the 59–55 Ma Ladybird granite suite. The eastern margin of the complex is bounded by the ductile-brittle east-dipping Slocan Lake–Champion Lakes normal fault system. The lower-plate of the Valhalla complex is characterized by Cretaceous to Eocene deformation, metamorphism, plutonism and an Eocene exhumation and cooling history. In contrast, the surrounding geology of the upper plate is characterized by Middle Jurassic deformation, metamorphism and plutonism, and a Mesozoic cooling history (Carr et al., 1987; Parrish et al., 1988; Simony and Carr, 1997).

The cross-sections shown in Figs. 3 and 4 depict the domed sheet-like geometry of the complex where approximately 5 km of structural relief is exposed. The 0.5–2 km thick Paleocene–Eocene Ladybird granite forms the upper sheet of Valhalla and Passmore domes; it overlies the Paleocene Airy quartz monzonite and contains an upward-increasing strain gradient related to the Valkyr–Slocan Lake extensional fault system. Beneath this is a 0.5–3 km sheet of metasedimentary rocks exposed on the flanks of Valhalla dome and the flanks and core of Passmore dome. Mapping and sampling of this unit is a particular focus of our study. It contains the Valhalla assemblage, a heterogeneous sequence of migmatitic pelitic schist, marble, calc–silicate gneiss, psammitic gneiss, metaconglomerate, quartzite, amphibolite and ultramafic rocks that may be correlative with part of the Paleozoic North American stratigraphic succession (Schaubs and Carr, 1998). The core of Valhalla dome comprises two ~0.5-km-thick sheets of the Early Cretaceous Mulvey granodiorite gneiss intercalated with 0.5–2-km-thick sheets of metasedimentary rocks. These deeper metasedimentary rocks do not have particularly distinctive lithologic sequences and are of uncertain affinity. South of Castlegar, the southern Valhalla complex consists of the Devonian Trail gneiss and paragneiss of uncertain affinity, overlain by Pennsylvanian metasedimentary rocks of the Mount Roberts Formation, all intruded by sheets of Early Cretaceous Kinnaird quartz monzonite and concordant swarms of Late Cretaceous China Creek pegmatites and Early Eocene Ladybird pegmatites (see Simony and Carr, 1997; Carr and Simony, 2000b). The pre-Eocene rocks of the complex exhibit structures that indicate a long-lived deformation history.

2.2. Dominant structures in Valhalla and Passmore domes

The predominant structure in the Valhalla and Passmore domes is an S_2 foliation that contains the peak metamorphic mineral assemblage and is concordant with the domal subculminations in the complex (Reesor, 1965; Schaubs and Carr, 1998; Figs. 2 and 5). It is concordant with transposed bedding (e.g. compositional variations within marbles), compositional layering, leucosomes, veins, dykes and other geologic contacts. In pelitic and semipelitic schists, S_2 is defined by platy minerals such as biotite, intergrown layers of biotite and sillimanite and discrete layers of sillimanite (Fig. 6a). In calc–silicate gneisses and amphibolites it is defined by the segregation of amphiboles and quartzo–feldspathic minerals and is parallel to compositional layering. In orthogneisses, such as the Mulvey granodiorite gneiss, S_2 is a gneissosity. S_2 contains the dominant lineation, L_2, a gently east- or west-plunging mineral lineation. Lineations are defined by sillimanite crystals, quartz ribbons and rare aligned biotite aggregates in semipelitic and pelitic schists, and by amphiboles in calc–silicate and amphibolite gneisses.

2.3. Folding

Four generations of folds were recognized in the Valhalla complex. There is evidence of early D_1 structures, overprinted by the S_2 foliation, such as quartz inclusion trails in garnet oriented at a high angle to S_2 (Fig. 6b) and isoclinal folds with fold hinges parallel to L_2. No early map-scale structures have been found, but, if correlations of the Valhalla assemblage with Paleozoic rocks of the Kootenay Arc are correct, then the Valhalla assemblage is inverted and may represent the upside-down limb of an early F_1 nappe (Schaubs and Carr, 1998). By analogy with structures such as the Riondel nappe and Carnes Creek nappe in the Kootenay Arc (Brown and Lane, 1988, and references therein) this deformation may be Jurassic or older.

F_2 and F_3 folds range in size from a few centimeters to several decameters and occur on the western side of Valhalla and Passmore domes. They are coaxial, affect leucosomes and the S_2 foliation, and postdate metamorphic mineral growth. F_2 folds are overturned, tight, and asymmetric, whereas F_3 folds are open to close and verge to the E–NE. F_3 folds have variable orientations but generally plunge moderately to shallowly W to NW with W- to SW-dipping axial planes. Map-scale F_2 and F_3 folds were not identified. F_4 folds are broad, tens-of-meter-scale open folds with steep axial planes. Millimeter-scale crenulations in semipelitic to pelitic schists may be related to D_4 deformation.

2.4. Downward increasing strain gradient — Late Cretaceous Gwillim Creek shear zone

High-strain zones that are concordant with S_2 occur at the base of both sheets of the Mulvey granodiorite gneiss in

Fig. 2. Geology of the Valhalla complex. Normal faults with top-side-down to the east displacement include: the brittle Champion Lakes fault (CLF), the ductile-brittle Columbia River (CRF) and Slocan Lake (SLF) fault zones and the ductile Valkyr shear zone (VSZ). The Gwillim Creek shear zones (GCSZ) are ductile thrust faults. Lines AA, BB and XX locate cross-sections shown in Figs. 3 and 4.

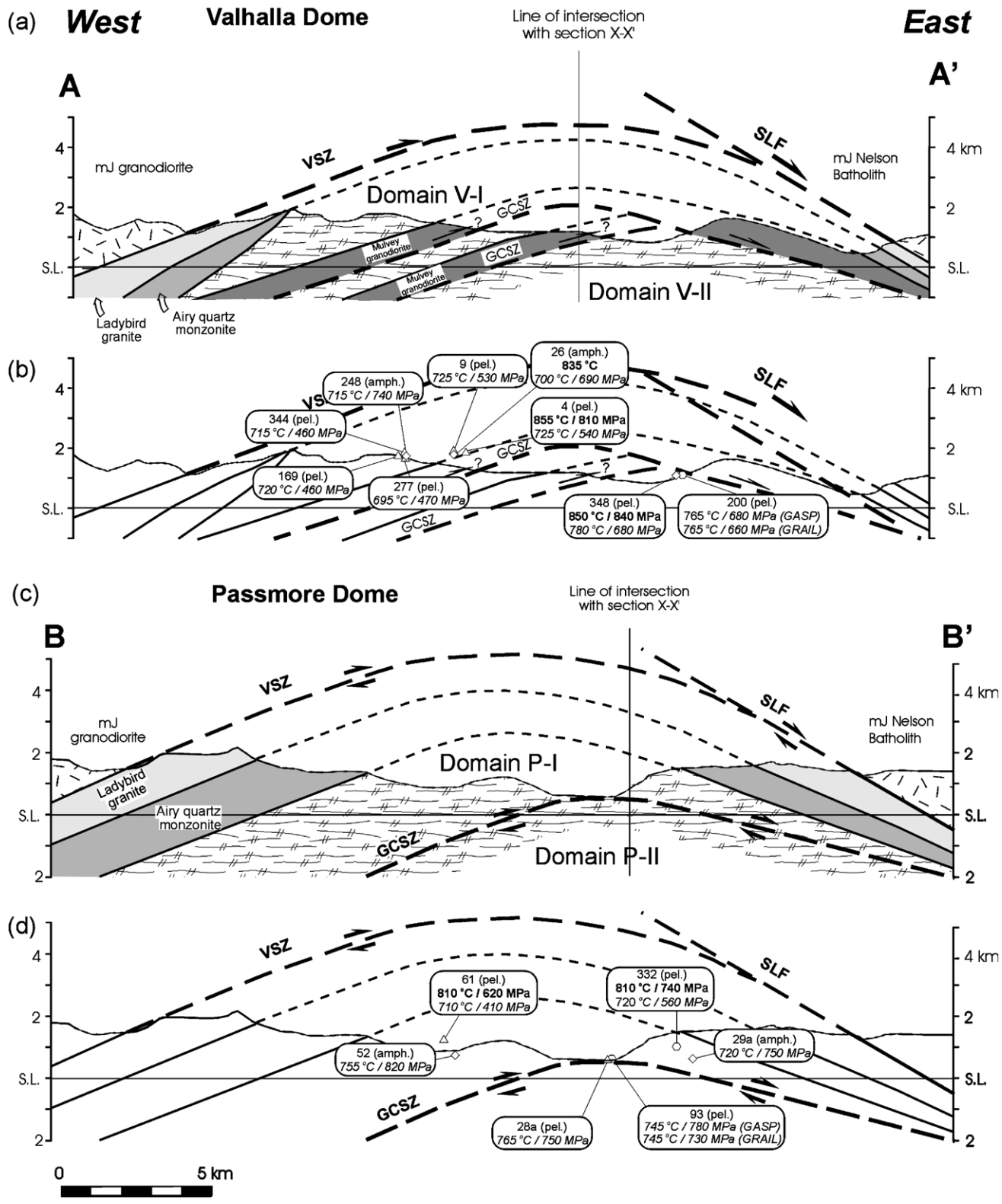

Fig. 3. Cross-sections through the northern Valhalla complex (see Fig. 2 for legend). (a) East–west cross-section of the Valhalla dome at the latitude of Gwillim Creek. (b) Same section, showing location of samples and results of thermobarometric calculations. (c) East–west cross-section through the Passmore dome. (d) Same section showing location of samples and results of thermobarometric calculations. Near-peak P–T calculations are in **bold**, and post-peak P–T calculations are in *italics.* Pressures for pelitic schists are calculated using the GASP equilibrium unless otherwise noted.

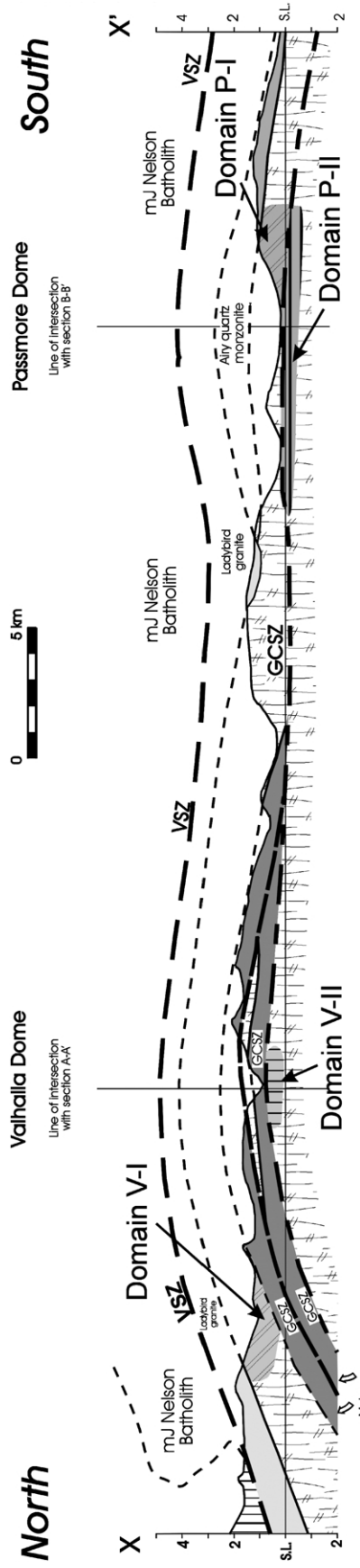

Fig. 4. North–south cross-section through the northern Valhalla complex outlining the structural domains.

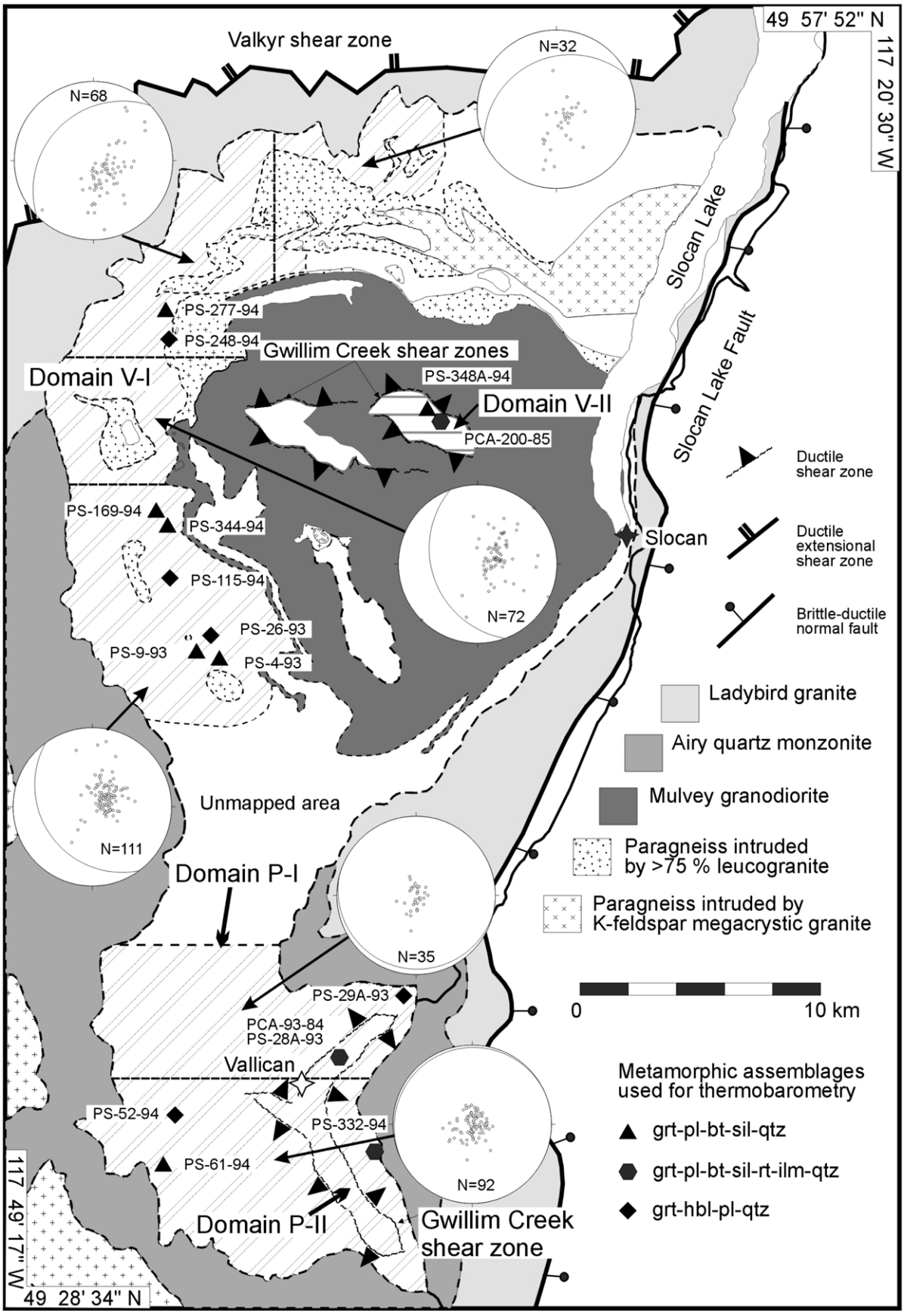
49 57' 52" N
117 20' 30" W
Valkyr shear zone
N=32
N=68
Slocan Lake
Slocan Lake Fault
PS-277-94
PS-248-94
Gwillim Creek shear zones
Domain V-I
PS-348A-94
Domain V-II
PCA-200-85
PS-169-94
PS-344-94
Slocan
PS-115-94
N=72
PS-26-93
PS-9-93
PS-4-93
Unmapped area
N=111
Domain P-I
N=35
PS-29A-93
PCA-93-84
PS-28A-93
Vallican
PS-52-94
PS-332-94
PS-61-94
N=92
Domain P-II
Gwillim Creek shear zone
117 49' 17" W
49 28' 34" N
Ductile shear zone
Ductile extensional shear zone
Brittle-ductile normal fault
Ladybird granite
Airy quartz monzonite
Mulvey granodiorite
Paragneiss intruded by >75 % leucogranite
Paragneiss intruded by K-feldspar megacrystic granite
0
10 km
Metamorphic assemblages used for thermobarometry
grt-pl-bt-sil-qtz
grt-pl-bt-sil-rt-ilm-qtz
grt-hbl-pl-qtz

Gwillim Creek in the core of Valhalla dome. They were recognized by Parrish et al. (1987), termed the Gwillim Creek shear zones (GCSZ), and interpreted as east-verging ductile thrust faults that duplicate map units. They are characterized by a strongly developed transposition foliation (S_T) and stretching lineation (L_T), boudins at the centimeter–decimeter scale, sheath folds and rootless isoclinal fold hinges (Schaubs and Carr, 1998). A significant reduction in grain size is observed within the lower 50 m of the granodiorite gneiss sheets. The Gwillim Creek shear zones are interpreted to merge into one zone of high strain in southern Valhalla dome, and extend southward beneath the Valhalla complex, cropping out as a zone of high strain with a downward increasing strain gradient in the core of Passmore dome (Schaubs and Carr, 1998) and in the China Creek culmination in the southern Valhalla complex (Simony and Carr, 2000). F_2 and F_3 folds at higher structural levels in the complex may be synchronous with deformation in the Gwillim Creek shear zone at lower levels, or deformation in the Gwillim Creek shear zone may have outlasted deformation at higher levels.

The Gwillim Creek shear zone is imaged in subsurface seismic reflection data at the latitude of Passmore dome, and has been interpreted as part of the Late Cretaceous thrust system that accommodated shortening in the Foreland thrust and fold belt (Parrish et al., 1987; Cook et al., 1988; Varsek and Cook, 1994; Carr, 1995; Cook and van der Velden, 1995; Simony and Carr, 2000).

2.5. Age of pre-Tertiary deformation

The southern Valhalla complex coincides with the southern end of the Shuswap metamorphic core complex where displacement on overprinting Eocene extensional shear zones is minimal. In this southern area the displacements on the Valkyr shear zone and Slocan Lake–Champion Lakes fault system are in the order of hundreds of meters to <2 km. Pre-Eocene structural relationships are also preserved and the transition from upper-crustal pre-Middle Jurassic structures to younger structures within the mid-crustal rocks is exposed (Simony and Carr, 1997; Carr and Simony, 2000a). Although there is evidence for a Paleozoic history (Simony, 1979; Simony et al., 1990), penetrative structures and foliations formed in the Middle Jurassic. They guided the intrusion of younger granitoids, and were, in part, reactivated at different structural levels in the Early Cretaceous, Late Cretaceous and/or Early Tertiary (Simony and Carr, 1997; Carr and Simony 2000b). Structural mapping of dated Paleozoic to Eocene granitoids has facilitated mapping the boundaries of these different-aged deformation zones. It is with these complexities and subtle overprinting relationships in mind that we approach the dating of structures in the northern Valhalla complex.

In Valhalla and Passmore domes, indirect evidence suggests that the rocks may have a Paleozoic and Middle Jurassic deformation history. If the correlation of the Valhalla assemblage with Paleozoic–Early Mesozoic North American and marginal basin stratigraphy is correct (Parrish, 1981; Schaubs and Carr, 1998), then cryptic Paleozoic tectonic boundaries are likely present within the supracrustal rocks, as well as Mesozoic or older F_1 nappes.

It is unclear when penetrative amphibolite-facies deformation and the formation of S_2 and S_T foliations started. A significant part of the strain is younger than the Early Cretaceous Mulvey granodiorite, and it is clearly older than the Eocene Ladybird granite suite which escaped penetrative deformation and is only deformed by Early Tertiary extensional shear zones. Detailed petrology and extensive geochronology studies were carried out on rocks in the core of Passmore dome by Parrish et al. (1988), Heaman and Parrish (1991) and Spear and Parrish (1996). They constrain the timing of the thermal peak of metamorphism at ~72–67 Ma. Evidence includes the age of diffusional high-temperature Pb-loss in monazite, the age of zircons in anatectic leucosome, the ages of monazites in pelitic schists and the age of a pegmatite which was recrystallized during the high-temperature event. The result is consistent with 73–65 Ma allanite and 61–56 Ma titanite high-temperature cooling ages from Early Cretaceous rocks. As the rocks have undergone ductile strain during high-temperature metamorphism, the age of metamorphism effectively dates at least part of the deformation in the core of Passmore dome (Parrish, 1995). F_2 and F_3 folds and deformation in the Gwillim Creek shear zone are compatible with one progressive deformation event.

3. Petrography and mineral chemistry

3.1. Sample locations and analytical strategy

Sixty samples of pelitic to semipelitic schist and 12 samples of amphibolite gneiss were collected from four geographic and structural domains (Fig. 5) in order to evaluate microstructures, metamorphic assemblages, metamorphic reaction textures and relative timing relationships between metamorphism and deformation. Domains V-I and P-I (Fig. 5) on the flanks of Valhalla and Passmore domes are made up of the Valhalla assemblage (Schaubs and Carr, 1998) and related supracrustal rocks. They are sandwiched between high strain zones of the overlying Eocene Valkyr shear zone and the underlying Late Cretaceous Gwillim

Fig. 5. Structure map of the northern Valhalla complex, focusing on the predominantly paragneiss of the Valhalla assemblage. Hatched areas indicate domains. Lower hemisphere equal-area projections illustrate poles to planes of the dominant S_2/S_T foliation. Great circles represent the mean orientation of this fabric. Straight dashed lines within domains delineate areas used for structural plots. Sample locations used for thermobarometric calculations are also shown.

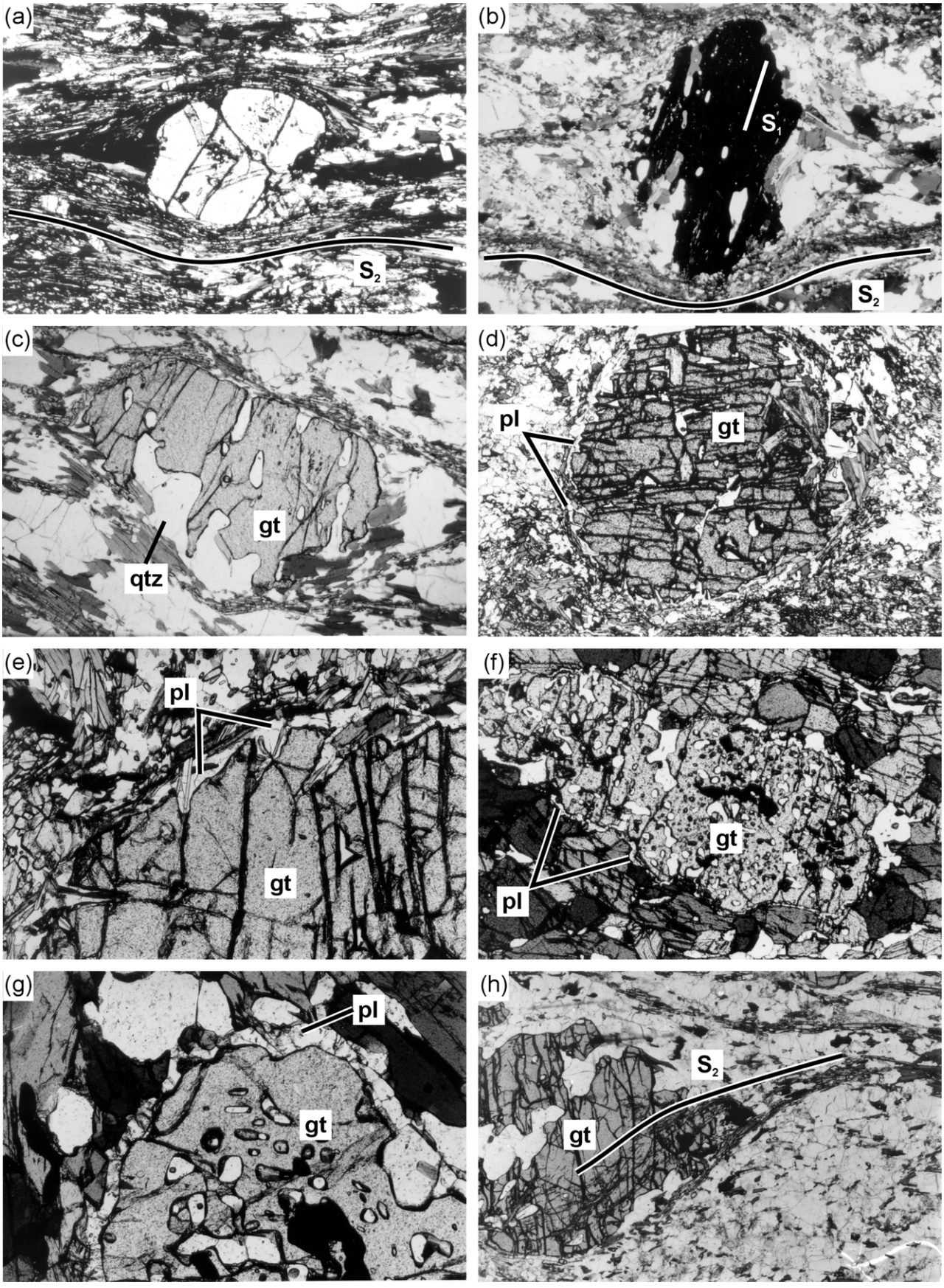
(a)
S2
(b)
S1
S2
(c)
gt
qtz
(d)
pl
gt
(e)
pl
gt
(f)
gt
pl
(g)
pl
gt
(h)
S2
gt

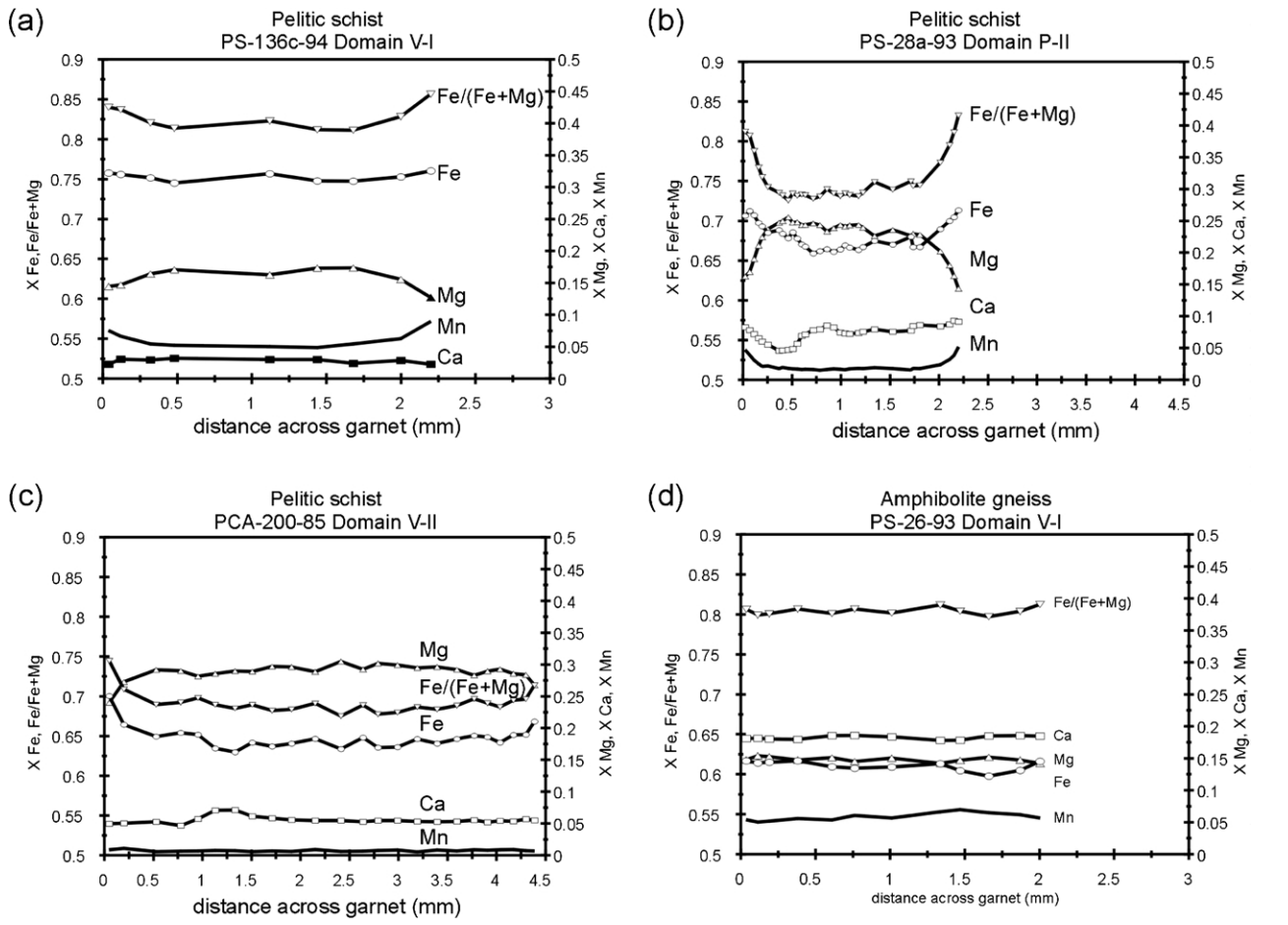

Fig. 7. Representative compositional zoning profiles of garnet from pelitic schists. (a) Zoning profile of garnet from upper sheet of metasedimentary rocks in Valhalla dome (domain V-I, sample PS-136c-94). (b) Zoning profile of garnet in pelitic schist from sheet of metasedimentary rocks in Passmore dome (domain P-II, sample PS-28a-93). (c) Zoning profile of garnet in pelitic schist from lower sheet of metasedimentary rocks in the core of the Valhalla dome (domain V-II, sample PCA-200-85). (d) Representative zoning profile of garnet from amphibolite gneiss in upper paragneiss sheet of Valhalla dome (domain V-I, sample PS-26-93).

Creek shear zone. The rocks display a well-developed S_2 foliation that has been affected by F_2 and F_3 folds on the western flanks of the complex. Domains V-II and P-II (Fig. 5) are situated within highly strained rocks of the 0.5–1-km-thick Gwillim Creek shear zone in the cores of Valhalla and Passmore domes, respectively, ~0.75–2 km structurally beneath domain I samples. The rocks contain a transposition foliation (S_T), a strong stretching lineation, and rootless and isoclinal folds. Petrology and geochronology of pelitic samples from domain P-II, primarily in the Passmore region, have previously been reported by Spear and Parrish (1996). Mineral compositions and zoning patterns were determined by electron microprobe analyses for 11 pelitic schist samples, and five amphibolite gneiss samples. X-ray composition maps were also used to reveal zoning patterns in some samples. Microstructures, reaction

Fig. 6. (a) Well developed S_2 fabric defined by peak metamorphic minerals biotite and sillimanite surrounding garnet in pelitic schist (domain V-I, sample PS-136c-94). Cross-polarized light; width = 4.8 mm. (b) Garnet porphyroblast with inclusions of quartz (S_i) from pelitic schist in Valhalla Dome (domain V-I, sample PS-21-93). Biotite and sillimanite foliation (S_2) wraps around garnet and occurs in pressure shadows. Cross-polarized light; width = 4.8 mm. (c) Garnet in pelitic schist from Valhalla dome (domain V-I, sample PS-19-93). Quartz embayments in garnet porphyroblast are produced during breakdown of garnet. Plane-polarized light; width = 2.4 mm. (d) Garnet in pelitic schist from Passmore dome (domain P-II, sample PS-28a-93). The garnet porphyroblast is surrounded by discontinuous reaction rim of fine-grained plagioclase. Polarized light; width = 4.8 mm. (e) Close-up view of Fig. 6d showing plagioclase reaction rim on garnet. Plane-polarized light; width = 0.96 mm. (f) Plagioclase rimming garnet porphyroblast in amphibolite gneiss from Passmore dome (domain P-I, sample PS-52-95). Plagioclase is interpreted to have formed during decompression via reaction (5). Plane-polarized light; width of 4.8 mm. (g) Close-up view of Fig 6f showing plagioclase reaction rim on garnet. Plane-polarized light; width = 0.96 mm. (h) Sillimanite and garnet from pelitic schist in lower paragneiss sheet within the core of Valhalla dome (domain V-II, sample PCA-200-85). Sillimanite inclusions in outer parts of garnet porphyroblast are aligned parallel with the external foliation and are continuous with aligned minerals in the pressure shadow. Plane-polarized light; width = 2.4 mm.

textures, and mineral zoning patterns summarized below represent a compilation of observations from all domains; differences between domains are noted.

3.2. Pelitic and semipelitic schist

Most pelitic schists contain the upper amphibolite-facies assemblage: quartz–biotite–plagioclase–garnet–sillimanite–potassium feldspar. Sillimanite may make up to 25% of some schists, but sillimanite–absent schists are also common. Accessory minerals include ilmenite, rutile, pyrite, zircon, apatite and monazite. Low-grade chlorite–quartz–albite–muscovite–calcite assemblages are restricted to late faults (e.g. Slocan Lake fault zone system), fractures and joint surfaces, and also occur locally within the Gwillim Creek shear zone, presumably due to late fluid infiltration.

Garnet, ranging from 0.5 mm to 2 cm in size, occurs as subhedral to anhedral porphyroblasts and poikiloblasts (Fig. 6a–d). The common occurrence of large quartz embayments (Fig. 6c), in association with reaction rims and pressure shadows composed of symplectitic biotite and quartz ± sillimanite, suggests retrograde operation of reaction (1):

$$\text{garnet} + \text{K-feldspar} + \text{melt} = \text{biotite} + \text{quartz} + \text{sillimanite} \quad (1)$$

In cases where sillimanite and biotite are not observed in close proximity to quartz embayments, this reaction may have resulted in growth of existing matrix grains rather than nucleation of new biotite and sillimanite grains.

Inclusions of quartz, biotite, plagioclase, sillimanite, apatite, ilmenite and rarely rutile commonly are concentrated without preferred orientation in garnet cores. Compositional differences were not detected between areas in garnet with high and low numbers of inclusions.

Microprobe analyses show garnet zoning patterns typical of those described by Tracy et al. (1976; type 3). Relatively flat profiles of Fe, Mg, Ca, and Mn are observed in most garnet cores (Fig. 7). In contrast to domain II samples, rims of most garnet in domain I samples display slightly lower (0.5–3 mol%) grossular contents. Sample PS-28a-93 (Fig. 7b) from domain P-II has a more calcic bulk composition and is more complexly zoned than other garnet porphyroblasts. A transect across the garnet (left to right in Fig. 7b) shows that grossular content decreases ~5 mol% into a trough, then increases 5 mol% to level off in the core, and finally increases ~1 mol% towards the other rim.

Some samples from all domains exhibit sharp 1–2 mol% increases of spessartine (X_{Mn}) towards the rim. In addition, garnet rims in contact with biotite have Fe/(Fe + Mg) ratios that are 0.05–0.08 higher relative to the core (Table 1 in Schaubs et al., 2001; see "Electronic Supplements" on the journal's homepage: http://www.elsevier.com/locate/jstrugeo). The outer ~0.5 mm of garnet rims in contact with quartz, plagioclase or potassium feldspar also display ~0.05 increases in Fe/(Fe + Mg) ratios relative to the garnet cores (Fig. 7), suggesting that retrograde zoning occurred in the presence of an effective intergranular exchange medium (hydrous fluid or melt). Garnet-rim zoning patterns described above could be produced by net-transfer reaction (1) or the reaction:

$$\text{garnet} + \text{K-feldspar} + H_2O = \text{biotite} + \text{sillimanite} + \text{plagioclase} \quad (2)$$

(Spear and Florence, 1992; Spear and Parrish, 1996), for samples, predominantly within domain II, in which plagioclase is present in reaction rims (Fig. 6d and e). Fe/(Fe + Mg) enrichment (0.03–0.04) of garnet rims in samples that lack sillimanite suggest modification by the Fe–Mg exchange reaction (Grt–Bt):

$$\text{almandine} + \text{phlogopite} = \text{pyrope} + \text{annite} \quad (3)$$

in the presence of an intergranular fluid.

Garnet cores and biotite in domain V-II generally have ~0.05–0.10 higher X_{Mg} relative to samples from other domains, reflecting a more Mg-rich bulk composition. Garnet cores are homogeneous and rims have Fe/(Fe + Mg) ratios ~5 mol% higher relative to the core (Fig. 7c).

The composition of matrix plagioclase grains in all samples that were analyzed ranges from An19 to 48 (Table 2 in Schaubs et al., 2001; see "Electronic Supplements" on the journal's homepage: http://www.elsevier.com/locate/jstrugeo). While individual plagioclase grains may be slightly heterogenous, systematic zoning was not observed. Within a single sample, X_{An} varies <0.05–0.10. In general, plagioclase grains in contact with garnet rims are slightly more calcic than matrix grains in domain I samples, and the reverse in domain II. Plagioclase inclusions in garnet from both domains are generally 3–5 mol% more calcic than plagioclase in the matrix or within intergrowths adjacent to garnet in the same sample.

Sample PS-28a-94 from domain P-II has well developed plagioclase reaction rims around garnet (Fig. 6d and e). Matrix plagioclase is consistently An = 50–52, and quartz inclusions within garnet have thin rims of plagioclase with An = 48. Plagioclase composition in reaction rims is heterogenous, varying from An = 37–51, but systematic variation with textural location was not discerned.

Biotite composition depends on location with respect to garnet (Table 3 in Schaubs et al., 2001; see "Electronic Supplements" on the journal's homepage: http://www.elsevier.com/locate/jstrugeo). Highest Ti concentrations (up to 10 mol) occur in matrix biotite and in biotite inclusions within quartz embayments interpreted to have been produced during garnet breakdown. Unarmoured biotite inclusions in garnet, and biotite in contact with and in the pressure shadows of garnet, have the lowest Fe/(Fe + Mg)

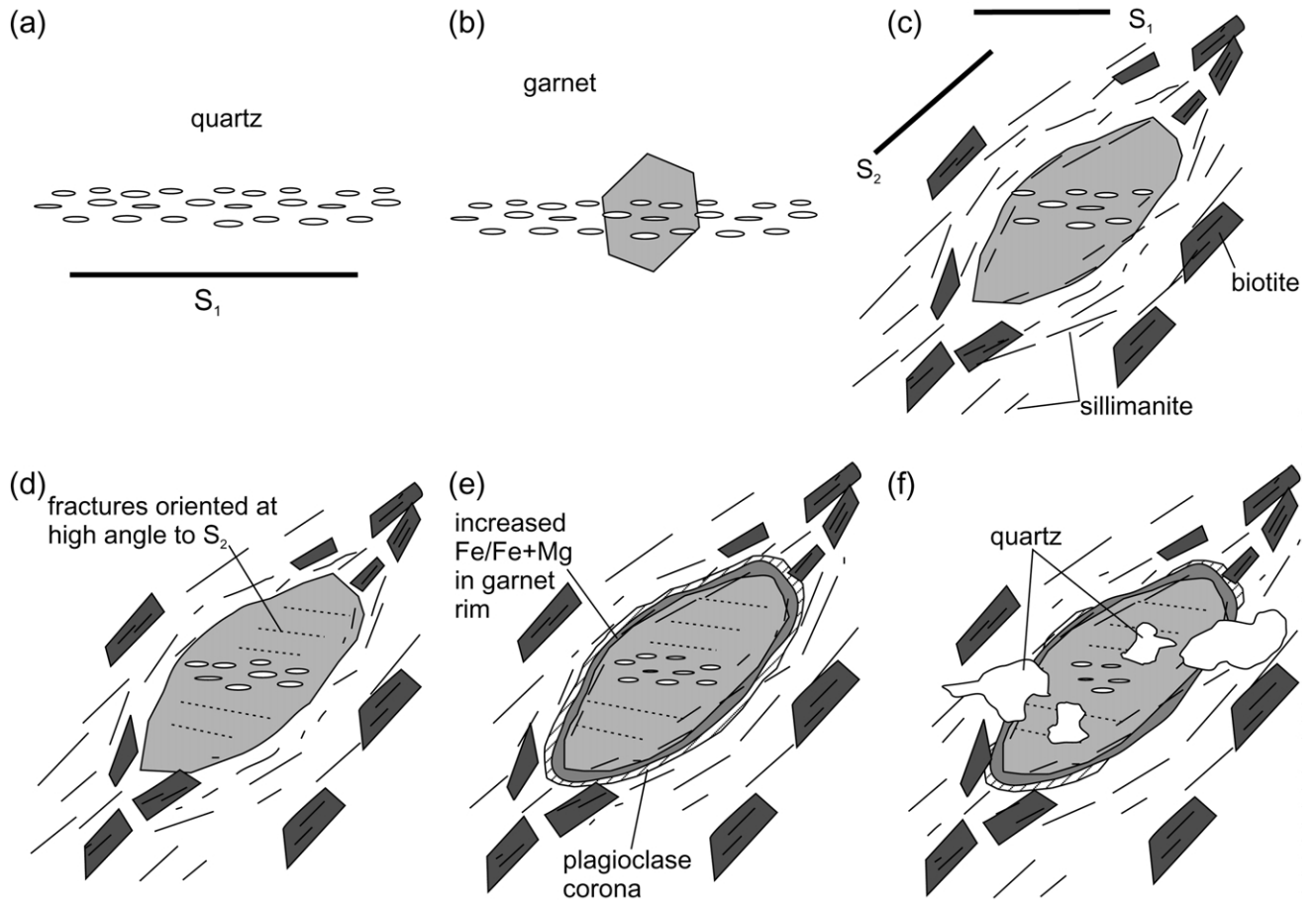

Fig. 8. Schematic illustrations outlining chronology of metamorphic and deformation events as deduced from petrographic observations and chemical data in pelitic schists. (a) S_1 formed and is defined by quartz inclusions. (b) Garnet overgrew S_1 fabric. (c) Garnet included sillimanite oriented in S_2/S_T indicating that S_2/S_T began to form during prograde metamorphism and garnet growth continued during S_2/S_T formation. Flat garnet profiles indicate garnet homogenization during thermal peak. (d) Garnet growth stopped while S_2 continued and wrapped around garnet porphyroblasts. (e) Garnet consumption caused increased Fe/(Fe + Mg) ratios around rim of garnet while plagioclase reaction rims formed around garnet. (f) Final garnet consumption formed vermicular quartz. Plagioclase reaction rims are diminished along garnet rims parallel to S_2 fabric due to continued deformation.

ratios (~0.45). Matrix biotite has the highest Fe/(Fe + Mg) ratios (~0.5).

Ilmenite and/or rutile are common in pelitic schists. In several samples where ilmenite and rutile coexist, textures are either ambiguous or they indicate that rutile overgrew ilmenite. This relationship can be accounted for by the GRAIL reaction:

$$\text{sillimanite} + 2\ \text{quartz} + 3\ \text{ilmenite} = \text{almandine} + 3\ \text{rutile} \quad (4)$$

which could be crossed either with increasing pressure on a prograde P–T path, or with near-isobaric cooling on a retrograde path. The occurrence of rutile overgrowths around ilmenite within the matrix, as opposed to within porphyroblasts, of sample PCA-200-85 (domain V-II) is most consistent with the latter alternative.

3.3. Amphibolite gneiss

Amphibolite gneisses, collected from domains V-I and P-I, vary in mineralogy, grain size and texture, reflecting protoliths with different bulk compositions. Most samples contain the assemblage: hornblende–plagioclase–quartz–ilmenite–garnet. Biotite, titanite, rutile and clinopyroxene also occur in some samples.

Garnet, up to 6 mm in diameter, is anhedral and frequently skeletal with quartz-filled embayments. Poikiloblastic garnet cores may contain up to 50% inclusions of quartz, hornblende and ilmenite. Plagioclase, which commonly forms partial to complete reaction rims around garnet (Fig. 6f and g), was probably produced by a reaction like:

$$\text{tschermakite–hornblende} + \text{garnet} + \text{quartz} = \text{tremolitic–hornblende} + \text{plagioclase} \quad (5)$$

Garnet porphyroblasts show flat compositional profiles with all components generally varying <3 mol%, and Fe/(Fe + Mg) increasing slightly (0.01–0.03) at rims (Fig. 7d; Table 4 in Schaubs et al., 2001; see "Electronic Supplements"

on the journal's homepage: http://www.elsevier.com/locate/jstrugeo). While most samples exhibit neglible zoning in CaO, one sample (PS-248-94) increases (Fig. 7d) and another (PS-52-94) decreases slightly (0.01–0.02) in X_{Ca} at garnet rims.

Plagioclase and quartz make up 20–35% of the rock and are usually nearly equal in modal abundance. Plagioclase compositions are heterogenous. Plagioclase within the matrix and within reaction rims around garnet varies in composition within a sample from An = 35–50, and An = 35–60, respectively (Table 5 in Schaubs et al., 2001; see "Electronic Supplements" on the journal's homepage: http://www.elsevier.com/locate/jstrugeo). In general, the most calcic grains are found in contact with garnet rims.

Most mafic gneisses in the Valhalla complex contain up to 65% equigranular, subhedral and euhedral hornblende. Hornblende in the matrix and in contact with garnet range from Fe/(Fe + Mg) ~ 0.45–0.58 in all samples (Table 6 in Schaubs et al., 2001; see "Electronic Supplements" on the journal's homepage: http://www.elsevier.com/locate/jstrugeo). Inclusions in sample PS-26-93 have lower Fe/(Fe + Mg) = ~0.41 than matrix hornblende (~0.45).

Biotite makes up to 30% of mafic gneisses. In some samples, biotite and hornblende are equal in proportion and both define the S_2 foliation. In other samples, biotite forms rims around hornblende and occurs along fractures in garnet. Biotite compositions within a sample are relatively homogeneous, with Fe/(Fe + Mg) varying <0.036 (Table 7 in Schaubs et al., 2001; see "Electronic Supplements" on the journal's homepage: http://www.elsevier.com/locate/jstrugeo).

Ilmenite, constituting up to 5% of mafic gneisses, occurs as equigranular, disseminated grains and as vermicular inclusions in garnet that may be surrounded by plagioclase reaction rims. Titanite and rutile are less common.

4. Timing relationships between metamorphism and deformation: relationships between microstructures and reaction textures

The microstructural, textural and chemical relationships described above provide evidence for a relative chronology of metamorphic reactions with respect to deformation events (Fig. 8). The earliest microstructures (S_1) are inclusion trails of quartz within garnet porphyroblasts (Figs. 6b and 8a); they are aligned at an angle to the external foliation, are finer grained than matrix grains and cannot be traced from the garnet to the matrix (Fig. 8b). Upper amphibolite-facies metamorphic minerals including sillimanite, biotite, K-feldspar and some garnets are aligned in the main S_2 (domains V-I and P-I) and S_T foliations (domains V-II and P-II) and in the pressure shadows of garnet. Sillimanite inclusions in garnet occur throughout all domains. They commonly occur within garnet rims, and are parallel to and continuous with the external foliation (Figs. 6h and 8c). These observations indicate that garnet porphyroblast growth and prograde amphibolite-facies metamorphism were ongoing during S_2/S_T formation.

Garnets are commonly oblate, and oriented at oblique angles to S_2/S_T. Although Spear and Parrish (1996) interpreted the shape to reflect modification due to ductile strain, this is unlikely because garnets fracture rather than deform by crystal–plastic processes (Passchier and Trouw, 1996). Rather, the shape may represent preferential growth in the flattening plane, and/or it may reflect preferential resorption in high strain areas during garnet breakdown reactions. The prevalence of oblate garnet in samples that do not have reaction rims favors the preferential growth hypothesis.

In general, the minerals that make up S_2 are deflected around garnet porphyroblasts indicating that S_2 and S_T formation outlasted garnet growth, the thermal peak of metamorphism (Fig. 8d), as well as the early stages of garnet breakdown. This is certainly the case within the Gwillim Creek shear zone where biotite and sillimanite produced by reactions (1) or (2) form part of the S_2/S_T. A similar relationship was inferred by Spear and Parrish (1996). All samples, including those from the Gwillim Creek shear zone, have shape fabrics indicative of high strain; however, microstructures such as straight grain boundaries, 120° boundaries between quartz grains, and the relatively large size and low number of internal subgrains in quartz indicate that the rocks annealed to some degree. These textures are in direct contrast to unannealed microstructures that are ubiquitous within Paleocene–Eocene Ladybird granite mylonites within the Early Tertiary Valkyr–Slocan Lake extensional fault zone system that bounds the upper margin of the Valhalla complex (Carr et al., 1987).

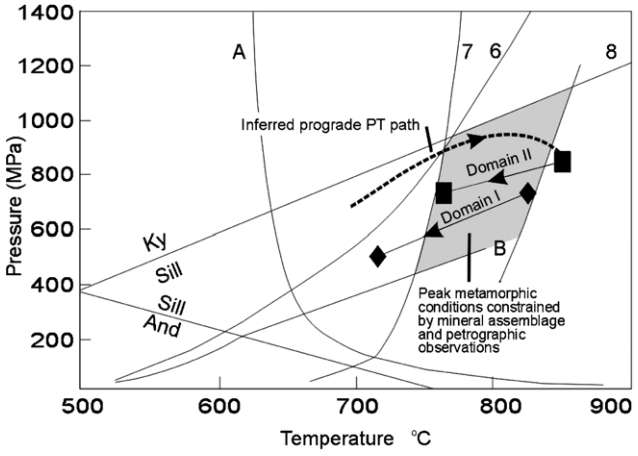

Fig. 9. Petrogenetic grid for pelitic schists showing important melt equilibria modified after Yardley (1989), Spear and Cheney (1989) and Spear (1993). Numbered equilibria correspond to those discussed in the text. Position of equilibrium (8) with X_{Fe} (biotite) = 0.5 from Spear and Parrish (1996). Additional equilibria: (A) albite + K-feldspar + quartz + H_2O = melt (Luth et al., 1964); (B) biotite + sillimanite + quartz = garnet + cordierite + K-feldspar + H_2O (Spear and Cheney, 1989).

Table 1
Thermobarometric data for pelitic schists

	Peak P–T			Post-peak P–T					
	GASP			GASP			GRAIL		
	T (°C)	P (MPa)	#	T (°C)	P (MPa)	#	T (°C)	P (MPa)	#
Domain V-I									
PS-4-94	855	810	1	725	540	1	–	–	–
PS-9-94	–	–	–	725	530	3	–	–	–
PS-169-94	–	–	–	720	460	2	–	–	–
PS-277-94	–	–	–	695	470	3	–	–	–
PS-344-94	–	–	–	715	460	2	–	–	–
Mean	855	810	1	715	490	11	–	–	–
Domain P-I									
PS-61-94	810	620	1	710	410	1	–	–	–
PS-332-94	810	740	2	720	560	3	725	680	1
Mean	810	680	3	715	485	4	725	680	1
V-I and P-I	825 ± 25	730 ± 10	4	715 ± 10	490 ± 50	15	725	680	1
Domain V-II									
PCA-200-85	–	–	–	765	680	1	765	660	1
PS-348a-94	850	840	1	780	680	2	–	–	–
Mean	850	840	1	775	680	3	765	660	1
Domain P-II									
PS-28a-93	–	–	–	765	750	2	–	–	–
PCA-93-84	–	–	–	745	780	2	745	730	2
Mean	–	–	–	755	770	4	745	730	2
V-II and P-II	850	840	1	765 ± 15	730 ± 50	7	755 ± 15	710 ± 15	3

The presence of biotite and sillimanite in proximity to continuous plagioclase reaction rims around garnets (Figs. 6d and e and 8e) suggests that reaction (2) was responsible for plagioclase production. The formation of quartz embayments (Figs. 6c and 8f) due to reaction (1) appears to have occurred at the same time or slightly after the formation of plagioclase reaction rims.

5. Pressure–temperature constraints

Metamorphic conditions are constrained by the following observations. The absence of muscovite, presence of sillimanite, garnet, potassium feldspar, and abundant evidence of in-situ melting restrict P–T conditions (Fig. 9) to the low pressure side of the kyanite = sillimanite equilibrium, and the high temperature sides of the vapor-absent melting reactions:

$$\text{muscovite} + \text{plagioclase} + \text{quartz} = \text{K-feldspar} + \text{sillimanite} + \text{melt} \quad (6)$$

$$\text{biotite} + \text{sillimanite} + \text{plagioclase} + \text{quartz} = \text{garnet} + \text{K-feldspar} + \text{melt} \quad (7)$$

(Lebreton and Thompson, 1987). The absence of orthopyroxene indicates that conditions were on the low-temperature side of the vapor-absent melting reaction:

$$\text{biotite} + \text{quartz} = \text{orthopyroxene} + \text{K-feldspar} + \text{melt} \quad (8)$$

(Vielzeuf and Clemens, 1992). These combined constraints indicate temperatures between approximately 780–850°C and pressure less than 1100 MPa. The observation of the assemblage corundum + sillimanite + potassium feldspar in a pegmatite within domain P-II aided Spear and Parrish (1996) in constraining temperatures within this domain to 820 ± 30°C.

Table 2
Thermobarometric data for amphibolite gneisses

	Peak P–T			Post-peak P–T		
	T (°C)	P (MPa)	#	T (°C)	P (MPa)	#
Domain V-I						
PS-26-93	835	–	1	700	690	1
PS-115-94[a]	790	770	1	–	–	–
PS-248-94	–	–	–	715	740	1
Mean	815	770	2	710	720	2
Domain P-I						
PS-29a-93	–	–	–	720	750	1
PS-52-94	–	–	–	755	820	2
Mean	–	–	–	740	790	3
V-I and P-I	815	770	2	725 ± 25	750 ± 50	5

[a] Post-peak garnet–hornblende temperatures considered unreliable due to extensive Fe–Mg reequilibration with biotite.

5.1. Geothermobarometry: analytical strategy

For each thin section, minerals were analyzed from two or more domains. For domains in which mineral compositions from similar textural locations varied <1%, compositions used in thermobarometric calculations represent averages. *P–T* data presented for each sample represent averages based on all domains within each thin section that exhibit similar textural relationships (Tables 1 and 2).

Pressures and temperatures were calculated with the computer program TWEEQU (Berman, 1991) using endmember thermodynamic data of Berman (1988, 1990) and Mader et al. (1994). Solution properties utilized included: garnet (Berman, 1990), biotite (McMullin et al., 1991), amphibole (Mader et al., 1994), and plagioclase (Aranovich, 1991). The latter model accounts for Al-avoidance in the mixing energetics and yields more reasonable pressures for sodic plagioclase (An15–30) than alternative models. In this study, we applied only the most robust thermometers and barometers (see below): the best constrained thermodynamically, with least insensitivity to errors in input data.

Locations of samples are shown in Fig. 5 and the results are projected into the planes of cross-sections shown in Fig. 3. Samples from the core of the dome (domain P-II) occur on the east side of Highway 6 near Vallican and Passmore, and replicate some of the samples studied by Spear and Parrish (1996).

5.1.1. Pelitic schists

Thermobarometric data for pelites were obtained for five samples from domain V-I, two from domain P-I, two from domain V-II and two from domain P-II (Fig. 5). *P–T* conditions were computed using the garnet–biotite thermometer (3), GRAIL barometer (4), and GASP barometer:

$$\text{grossular} + 2\ \text{sillimanite} + \text{quartz} = 3\ \text{anorthite} \quad (9)$$

Fixed activities for ilmenite were calculated assuming ideal site mixing (Table 8 in Schaubs et al., 2001).

In this study, pressure and/or temperatures have been calculated for: (1) *near-thermal peak* using compositions of armoured biotite inclusions, garnet cores, and matrix plagioclase; and (2) *post thermal-peak* conditions using compositions of garnet rims and proximal (~0.1–1 mm) biotite, plagioclase, and ilmenite grains that are separated from garnet by non-ferromagnesium minerals.

5.1.2. Amphibolite gneiss

Five samples of amphibolite gneiss (three from domain V-I, and two from domain P-I) were studied (Figs. 3 and 5; Table 2). As no armoured hornblende inclusions were observed in garnet, *near thermal-peak* conditions have been calculated from garnet core and matrix mineral compositions for two samples with garnet porphyroblasts that are only partly surrounded by hornblende or biotite. *Post thermal-peak* conditions have been calculated from garnet rims and adjacent hornblende and plagioclase.

P–T conditions were computed using the garnet–biotite thermometer (3), garnet–hornblende thermometer:

$$5\ \text{almandine} + 3\ \text{tremolite} = 3\ \text{Fe-tremolite} + 5\ \text{pyrope} \quad (10)$$

and the GHPS barometer:

$$12\ \text{anorthite} + 3\ \text{tremolite} = 4\ \text{grossular} + 2\ \text{pyrope} + \text{tschermakite} + 12\ \text{quartz} \quad (11)$$

5.2. Thermobarometric results: near-thermal peak conditions

Average near-peak conditions for pelitic rocks of domain I are 825°C and 730 MPa (Table 1), based on (a) two armoured biotite inclusions in garnet porphyroblasts (samples 61-94 and 332-94), and (b) matrix biotite and the core of a garnet porphyroblast from a part of sample 4-94 with no sillimanite. The lack of sillimanite suggests that minimal Fe-enrichment in matrix biotite would have occurred due to retrograde garnet breakdown via equilibrium (1) or (2), as discussed by Spear and Florence (1992) and Spear and Parrish (1996). Near-peak conditions of 815°C and 770 MPa, calculated for two amphibolite samples (Table 2), are in good agreement with the pelite results.

Calculated near-peak conditions for one sample in domain V-II with an armoured biotite inclusion are 850°C and 840 MPa. Although this result matches the upper temperature limit provided by the absence of orthopyroxene in these rocks, we cannot rule out the possibility that transient temperatures may have been slightly higher, possibly due to frictional heating within the shear zone (e.g. Camacho et al., 2001), in order to have produced sapphirine–quartz–garnet–assemblages reported from one locality (Simandl et al., 2000). Our calculated values compare well with Spear and Parrish's (1996) determination of a 800 ± 100 MPa pressure range for all samples and near-peak temperatures of 810–836°C for one sillimanite-free sample in domain P-II. The 120 MPa difference measured between domains I and II corresponds reasonably with the structural position of samples in domain II ~2 km below those in domain I.

5.2.1. P–T results: post thermal-peak temperatures on the flanks of Valhalla and Passmore domes (domains V-I and P-I)

P–T results from subdomains within a thin section as well as from different samples from the same locality yield replicable results (e.g. PS-4-93 and PS-9-93 from Mount Rinda and PS-169-94 and PS-344-94 from the headwaters of Bannock Burn Creek; Table 1). In the case of sample PS-332-94 from Slocan Ridge on the eastern flank of Passmore

dome, the GRAIL barometer yields ~120 MPa higher pressure than the GASP barometer. This discrepancy does not appear to be related to calibration error, as both barometers return very similar pressures in domain II (Table 1). As most samples examined in both domains do not have rutile, GRAIL results are not utilized in averages or comparisons below. Taking the Valhalla and Passmore data sets together (domains V-I and P-I), temperatures range from 695 to 725°C and pressures from 410 to 560 MPa, with average conditions of 715°C and 490 MPa. There is no apparent geographic pattern to these results from samples within a 2-km-thick structural section, and the small range is well within the overall uncertainty of the thermobarometric calculations. Structural and microstructural observations summarized above indicate that these are the conditions under which at least part of the Late Cretaceous penetrative deformation occurred throughout Valhalla and Passmore domes.

P–T results for amphibolite gneisses from domains V-I and P-I yield average conditions of 725°C and 750 MPa, (Table 2) based on amphibole equilibria (10) and (11). Whereas this average temperature concurs with that derived from the pelites, the pressure is 260 MPa higher than recorded by the pelite samples. Even allowing for the possibility of calibration errors that could make pressures determined from equilibrium (11) systematically ~100 MPa too high, the much larger discrepancy suggests that the amphibolite assemblage likely did not reequilibrate at lower pressures during cooling, either due to limited access of catalyzing fluids or because of sluggish kinetics of the amphibolite reaction assemblage.

Garnet–biotite (equilibrium 3) temperatures for some amphibolite samples are 60–100°C higher than garnet–hornblende temperatures (equilibrium 10). In these samples, biotite occurs as rims on hornblende, making both phases susceptible to retrograde Fe–Mg exchange that would shift equilibrium (3) to higher temperature and equilibrium (10) to lower temperature. As biotite is modally less abundant (10–15%) than hornblende (40–50%), garnet–biotite temperatures would be affected more than garnet–hornblende temperatures, but we cannot rule out that hornblende–garnet temperatures reported in Table 2 were also affected somewhat by this process. In the light of these problems with amphibolite samples, and because amphibolites are absent within domain II, only *P–T* results for pelitic rocks are used in interdomain comparisons discussed below.

5.2.2. P–T results: post-thermal-peak conditions for the Gwillim Creek shear zone in the cores of Valhalla and Passmore domes (P-II and V-II)

P–T conditions for domain II, calculated from proximal garnet and biotite rims that are separated by either quartz or plagioclase, range between 745 and 780°C and 680 and 780 MPa and average 765°C and 730 MPa (Table 1), with good agreement between GRAIL and GASP barometers. Domain V-II samples show ~15°C higher temperatures and 100 MPa lower pressures than domain P-II samples, but these differences are within the overall uncertainties of the calculations. Results for domain P-II samples are identical to the upper values of the range (690–750°C) reported by Spear and Parrish (1996). The overall slightly higher temperatures determined in this study may result from microprobe analysis of spots slightly further away from garnet rims, that ubiquitously display rimward increasing Fe/(Fe + Mg).

5.2.3. Summary of P–T results

P–T calculations summarized above indicate no significant differences in pressure or temperature between the Valhalla and Passmore areas in either domain I or in the structurally lower domain II. Calculated near-peak *P–T* conditions are ~825°C and 730 MPa for domain I, compared with ~850°C and 840 MPa for domain II. Post thermal-peak conditions recorded by pelitic schists average ~715°C and 490 MPa for domain I, compared with 765°C and 730 MPa domain II, both consistent with petrographic observations that indicate that retrograde operation of reaction (2) occurred above the stability field of muscovite. Although the near-peak pressure difference (120 MPa) between domains I and II is compatible with their present relative structural positions, the post-peak pressure difference (230 MPa) between domains is considerably larger. As the post thermal-peak *P–T* values likely reflect the conditions at which reaction (2) was quenched (Spear and Parrish, 1996), the apparent differences in post-peak conditions suggest contrasting post-peak cooling histories between the two domains. Using the average values quoted above, cooling trajectories are 14 and 25°C/km for domains I and II, respectively. The more rapid cooling per kilometer of exhumation, as well as reaction (2)'s higher quenching temperature in domain II relative to domain I are consistent with a model in which the high temperature cooling history was controlled by juxtaposition of domain II rocks against a cold footwall during exhumation. This model was one alternative considered by Spear and Parrish (1996) in order to account for potentially very rapid cooling rates (3–80 or 200–2500°C/Ma, depending on diffusivity data used) determined by thermal modeling of apparent temperatures measured for biotite inclusions in garnet porphyroblasts from domain P-II.

The observed similarity in composition between plagioclase inclusions in garnet and matrix plagioclase led Spear and Parrish (1996) to conclude that the retrograde *P–T* path for domain P-II was roughly parallel to isopleths for garnet–plagioclase equilibria (e.g. GASP = ~1.5 MPa/°). The average retrograde *P–T* path calculated for domain II samples is slightly less (~1.3 MPa/°) than this value, suggesting that the more calcic garnet rims and the more sodic plagioclase found in contact with garnet rims in some samples may have been produced as isopleths of reaction (2) were crossed during cooling. Additional support for a shallower retrograde *P–T*

path in domain II is provided by the rare occurrence of rutile overgrowths on ilmenite (sample PCA-200-85 in domain V-II), which suggests that a portion of the P–T path may have been shallower than isopleths of the GRAIL equilibrium (~0.75 MPa/°).

The calculated retrograde P–T path for domain I (~2.2 MPa/°) is significantly greater than the slope of garnet–plagioclase equilibria, consistent with less calcic garnet rims and slightly more calcic plagioclase in contact with garnet rims in most pelitic samples of this domain. In amphibolites, as well, the occurrence of the most calcic plagioclase within reaction rims around garnet is consistent with a steeper retrograde P–T path than the 1.3 MPa/° calculated slope of reaction (11).

The occurrence of slightly more sodic plagioclase in the core of one garnet porphyroblast relative to matrix plagioclase led Spear and Parrish (1996) to suggest that the prograde P–T path for domain II may have involved earlier higher pressures or near-isobaric heating. In contrast to the inclusion they analyzed, all plagioclase inclusions analyzed in this study from both structural domains are more calcic than matrix plagioclase, suggesting a prograde P–T path steeper than garnet–plagioclase isopleths. Combined with the above constraints on the retrograde P–T path, the data suggest a compressed, clockwise P–T path without a segment of near isothermal decompression. This type of P–T path is consistent with metamorphism having occurred in response to crustal thickening that was rapidly followed by extensional denudation.

6. Conclusions and discussion

The metamorphic and deformation history preserved in supracrustal rocks is consistent throughout all structural levels within Valhalla and Passmore domes in the northern Valhalla complex. Peak mineral assemblages define the predominate S_2/S_T foliation, and sillimanite inclusions in garnet aligned with the external foliation indicate that garnet porphyroblast growth, prograde amphibolite-facies metamorphism and in situ melting were ongoing during S_2/S_T deformation. Progressive foliation formation outlasted garnet growth, the thermal peak of metamorphism and early stages of garnet breakdown. Intense strain (S_T) in the Gwillim Creek shear zone, exposed at the deepest exposed structural levels in both domes, was synchronous with and outlasted penetrative deformation (S_2) throughout the northern complex.

Temperature and pressure data indicate near-peak conditions of ~825°C and 730 MPa for domain I, compared with ~850°C and 840 MPa for domain II. Post thermal-peak conditions recorded by pelitic schists average ~715°C and 490 MPa for domain I, compared with 765°C and 730 MPa for domain II. Taken together with microstructural data, these data indicate the conditions at which most of the penetrative S_2 deformation throughout the northern Valhalla complex and in the Gwillim Creek shear zone (S_T) at lower structural levels occurred. Although our data do not constrain absolute cooling rates, they do suggest a possible difference in cooling history between the two structural domains. More rapid cooling of domain II relative to domain I during exhumation is compatible with conductive cooling during thrusting of the northern Valhalla complex onto a cold footwall, a model suggested by Spear and Parrish (1996) to account for potentially very rapid cooling rates determined petrologically. This relationship cannot be accounted for in models of ductile thinning, tectonic exhumation or rapid erosion. The thrust model also allows a mechanism of cooling the rocks by 200–300°C, and keeping them in the middle crust above greenschist-facies for ca. 10 Ma until intrusion of the ca. 59–56 Ma Ladybird granite suite just prior to exhumation in the Early Tertiary on the Valkyr–Slocan Lake extensional shear zone system.

The relationship between metamorphic reactions, reaction textures and S_2 on the flanks of Valhalla and Passmore domes is the same as the relationship between metamorphic reactions, reaction textures and S_T in the Gwillim Creek shear zone in the cores of both domes. Therefore, we conclude that metamorphism and a significant part of progressive penetrative D_2 (S_2/S_T) deformation throughout the northern complex occurred during one event. The 72–67 Ma age of deformation and metamorphism established by Spear and Parrish (1996) for rocks near Vallican in the Passmore dome can be extrapolated throughout the northern Valhalla complex placing timing constraints on D_2 and accompanying metamorphism as predicted by Parrish (1995). The inferred clockwise P–T path suggests crustal thickening as the heat source for metamorphism, consistent with the paucity of Late Cretaceous plutons.

The ca. 70 Ma culmination of progressive penetrative deformation and metamorphism throughout the northern Valhalla complex coincides with the major period of shortening in the Foreland belt (Price, 2000). To the east of Valhalla, structures in the eastern part of the Omineca belt in the Kootenay Arc and Purcell Anticlinorium are Middle Jurassic, and formed during orogenesis related to the accretion of the Intermontane Superterrane to the western margin of North America. These structures are cut by ca. 100 Ma plutons and were exhumed in the Early Cretaceous (Archibald et al., 1983). *If* strain in the Valhalla complex *is directly linked to shortening* in the Foreland belt, then displacement must be transferred eastward beneath the eastern Omineca belt, as suggested by Varsek and Cook (1994) and Cook and van der Velden (1995). This transfer could be accommodated by deformation in the Valhalla complex; Cook and ver der Velden correlated the Gwillim Creek shear zone with the 'K-reflectors' that form the roof of a duplex that merges with the Rocky Mountain basal detachment beneath the Purcell Anticlinorium.

Tectonic models such as these have been questioned by Williams (1999) who argued that ductile thrust sheets are

inconsistent with the style of structures and ductile flow in the middle crust. In an attempt to revise tectonic models, Brown (2001) modeled the Omineca and Foreland belts as an orogenic wedge that behaved in terms of critical taper theory. Deformation in the hinterland may have changed the geometry of the orogenic taper, thus indirectly causing thrusting in the Foreland belt (Williams, 1999; Brown, 2001); however, this model does not require direct linkage of particular hinterland and foreland structures. In the hinterland, progressive deformation may occur throughout the thickening wedge; high strain zones in deep-seated rocks may be transient and migrate downward as the wedge advances. Progressive thickening of the wedge may be accommodated by downward migration of shear, incorporating footwall rocks into the wedge. Concomitant denudation and exhumation of rocks may be going on in other parts of the wedge to approach or maintain a critical taper. This interpretation is not inconsistent with data from the Valhalla complex. In this scenario, the zone of Late Cretaceous metamorphism and penetrative deformation in Valhalla complex would represent a transient shear zone. High strain and more rapid cooling at the lowest structural level in the complex may indicate its location at the base of the wedge as it advanced eastward onto cold basement.

Acknowledgements

We are grateful to Cordilleran colleagues for discussions related to this project, particularly Philip Simony and Paul Williams. The paper benefited from constructive reviews from Ed Ghent and Wouter Bleeker. The research was supported by a NSERC Research grant to Carr, and Schaubs was supported by financial assistance from Carleton University.

References

Aranovich, L.Y., 1991. Mineral Equilibria of Multicomponent Solid Solutions. Nauka Press, Moscow 253pp.

Archibald, D.A., Glover, J.K., Price, R.A., Farrar, E., Carmichael, D.M., 1983. Geochronology and tectonic implications of magmatism and metamorphism, southern Kootenay Arc and neighbouring regions, southeastern British Columbia; Part I, Jurassic to mid-Cretaceous. Canadian Journal of Earth Sciences 20, 1891–1913.

Berman, R., 1988. Internally-consistent thermodynamic data for stoichiometric minerals in the system Na_2O–K_2O–CaO–MgO–FeO–Fe_2O_3–Al_2O_3–SiO_2–TiO_2–H_2O–CO_2. Journal of Petrology 29, 445–522.

Berman, R., 1990. Mixing properties of Ca–Mg–Fe–Mn garnets. American Mineralogist 75, 328–344.

Berman, R., 1991. Thermobarometry using multiequilibrium calculations: a new technique with petrologic applications. Canadian Mineralogist 29, 833–855.

Brown, R.L., 2001. Thrust belt accretion and hinterland underplating of orogenic wedges: An example from the Canadian Cordillera. American Association of Petroleum Geologists, McClay, K. (Ed.). Accepted.

Brown, R.L., Carr, S.D., Johnson, B.J., Coleman, V.J., Cook, F.A., Varsek, J.L., 1992. The Monashee décollement of the southern Canadian Cordillera: a crustal scale shear zone linking the Rocky Mountain Foreland Belt to lower crust beneath accreted terranes. In: McClay, K. (Ed.). Thrust Tectonics. Chapman & Hall, London, pp. 357–364.

Brown, R.L., Lane, L.S., 1988. Tectonic interpretation of west-verging folds in the Selkirk Allochthon of the southern Canadian Cordillera. Canadian Journal of Earth Sciences 25, 292–300.

Camacho, A., McDougall, I., Armstrong, R., Braun, J., 2001. Evidence for shear heating, Musgrave Block, Central Australia. Journal of Structural Geology 23, 1007–1013.

Carr, S.D., 1991. Three crustal zones in the Thor–Odin–Pinnacles area, southern Omineca Belt, British Columbia. Canadian Journal of Earth Sciences 28, 2003–2023.

Carr, S.D., 1995. The southern Omineca Belt, British Columbia: new perspectives from the Lithoprobe geoscience program. Canadian Journal of Earth Sciences 32, 1720–1739.

Carr, S.D., Simony, P.S., 2000. Relationship between Middle Jurassic and Cretaceous to Middle Eocene deformation and plutonism in mid-crustal rocks of the Omineca Belt, southern Canadian Cordillera. Geological Society of Australia, 15th Australian Geological Convention. Sydney July 3–7, 2000. Abstracts no. 59, p. 72.

Carr, S.D., Simony, P.S., 2000. Plutons and tectonics; compression, extension and the Valhalla core complex in southeastern British Columbia. GeoCanada 2000, Calgary, Alberta. Pre-meeting Field Trip Guidebook No. 9, May 25–28, 2000.

Carr, S., Parrish, R., Brown, R., 1987. Eocene structural development of the Valhalla complex, Southeastern British Columbia. Tectonics 6, 175–196.

Cook, F., Van der Velden, A., 1995. Three-dimensional crustal structure of the Purcell Anticlinorium in the Cordillera of southwestern Canada. Geological Society of America Bulletin 107, 642–664.

Cook, F., Green, A., Simony, P., Price, R., Parrish, R., Milkereit, B., Brown, R., Coflin, K., Patenaude, C., 1988. Lithoprobe seismic reflection structure of the southeastern Canadian Cordillera: initial results. Tectonics 7, 157–180.

Cook, F., Varsek, J., Clowes, R., Kanasewich, E., Spencer, C., Parrish, R., Brown, R., Carr, S., Johnson, B., Price, R., 1992. Lithoprobe crustal reflection cross section of the southern Canadian Cordillera, 1. Foreland thrust and fold belt to Fraser river fault. Tectonics 11, 12–35.

Crowley, J.L., Ghent, E.D., Carr, S.D., Simony, P.S., Hamilton, M.A., 2000. Multiple thermotectonic events in a continuous metamorphic sequence, Mica Creek area, southeastern Canadian Cordillera. Geological Materials Research 2, 1–45.

Crowley, J.L., Brown, R.L., Parrish, R.R., 2001. Diachronous deformation and a strain gradient beneath the Selkirk allochthon, northern Monashee complex, southeastern Canadian Cordillera. Journal of Structural 23, 1103–1121.

Digel, S.G., Ghent, E.D., Carr, S.D., Simony, P.S., 1998. Early Cretaceous kyanite–sillimanite metamorphism and Paleocene sillimanite overprint near Mount Cheadle, southeastern British Columbia: geometry, geochronology, and metamorphic implications. Canadian Journal of Earth Sciences 35, 1070–1078.

Gibson, H.D., Brown, R.L., Parrish, R.R., 1999. Deformation-induced inverted metamorphic field gradients: and example from the southeastern Canadian Cordillera. Journal of Structural Geology 21, 751–767.

Heaman, L., Parrish, R., 1991. Uranium–lead geochronology of accessory minerals. In: Heaman, L., Ludden, J. (Eds.). Applications of Radiogenic–Isotope System to Problems in Geology. Short Course Serial, Mineralogical Association of Canada 19, pp. 82–102.

Johnson, B.J., 1994. Structure and tectonic setting of the Okanagan Valley fault system in the Shuswap lake setting, southern British Columbia. Ph.D. thesis, Carleton University, Ottawa, Ontario.

LeBreton, N., Thompson, A.B., 1987. Fluid-absent (dehydration) melting of biotite in metapelites in the early stages of crustal anatexis. Contributions to Mineralogy and Petrology 99, 226–237.

Little, H.W., 1960. Nelson map-area, west half, British Columbia. Geological Survey of Canada Memoir 308.

Luth, W., Jahns, R., Tuttle, O., 1964. The granite system at pressures of 4 to 10 kbars. Journal of Geophysical Research 69, 659–773.

Mader, U.K., Percival, J.A., Berman, R.G., 1994. Thermobarometry of garnet–clinopyroxene–hornblende granulites from the Kapuskasing structural zone. Canadian Journal of Earth Science 31, 1134–1145.

McMullin, D.W.A., Berman, R.G., Greenwood, H.J., 1991. Calibration of the SGAM thermobarometer for pelitic rocks using data from phase-equilibrium experiments and natural assemblages. In: Gordon, T.M., Martin, F.R. (Eds). Quantitative methods in petrology; an issue in honor of Hugh J. Greenwood. The Canadian Mineralogist 29, 889–908.

Parrish, R.R., 1981. Geology of the Nemo Lakes Belt, northern Valhalla Range, Southeast British Columbia. Canadian Journal of Earth Sciences 18, 944–958.

Parrish, R., 1995. Thermal evolution of the Southeastern Canadian Cordillera. Canadian Journal of Earth Sciences 32, 1618–1642.

Parrish, R.R., Price, R.A., Carr, S.D., 1987. Late Cretaceous–Paleogene metamorphism in the core zone of the Cordilleran orogen: Valhalla complex of southeastern British Columbia. Geological Society of America, Program with Abstracts 19, 800.

Parrish, R., Carr, S., Parkinson, D., 1988. Eocene extensional tectonics and geochronology of the southern Omineca Belt, British Columbia and Washington. Tectonics 7, 181–212.

Passchier, C.W., Trouw, R.A.J., 1996. Microtectonics. Springer, Berlin.

Price, R.A., 2000. The evolution of the southern Canadian foreland thrust and fold belt and the kinematics of Cordilleran orogenesis, GAC Abstracts, GeoCanada 200-Millennium Geoscience Summit-Conference CD.

Price, R.A., Mountjoy, E.W., 1970. Geologic structure of the Canadian Rocky Mountains between Bow and Athabasca rivers — a progress report. Geological Survey of Canada, Special Paper 6, 7–25.

Reesor, J.E., 1965. Valhalla gneiss complex, British Columbia. Geological Survey of Canada, Bulletin, 129.

Scammell, R.J., 1993. Mid-Cretaceous to Tertiary thermotectonic history of former mid-crustal rocks, southern Omineca Belt, Canadian Cordillera. Ph.D. thesis, Queen's University, Kingston, Ontario.

Schaubs, P., 1995. Stratigraphic and metamorphic constraints on the tectonic evolution of the Valhalla complex, southern British Columbia. M.Sc. thesis, Carleton University, Ottawa, Ontario.

Schaubs, P., Carr, S., 1998. Geology of metasedimentary rocks and late Cretaceous deformation history, in the Northern Valhalla complex, British Columbia. Canadian Journal of Earth Sciences 38, 1018–1036.

Schaubs, P., Carr, S., Berman, R., 2001. Data repository for extra tables and figures. http://www.ned.dem.csiro.au/unrestricted/SchaubsPeter/valhalla; http://www.elsevier.com/locate/jstrugeo

Simandl, G.J., Marshall, D., Laird, J., 2000. Gem-quality cordierite deposits, Slocan Valley, British Columbia (NTS 82F/12E). In: Geological Fieldwork 1999, British Columbia Geological Survey Paper 2000-1, pp. 349–358.

Simony, P., 1979. Pre-carboniferous basement near Trail, British Columbia. Canadian Journal of Earth Sciences 16, 1–11.

Simony, P.S., Carr, S.D., 1997. Large lateral ramps in the Eocene Valkyr Shear Zone: extensional ductile faulting controlled by plutonism in southern British Columbia. Journal of Structural Geology 19, 769–784.

Simony, P.S., Carr, S.D., 2000. Geometry and timing of a Late Cretaceous compressional ductile shear zone in the Valhalla core complex: inversion of a large lateral thrust ramp. GAC Abstracts, GeoCanada 200-Millennium Geoscience Summit-Conference CD.

Simony, P., Armstrong, R.L., Mortenson, J.R., Van der Heyden, P., 1990. Geochronometry of a Devonian pluton in the Trail Gneiss north of Trail, British Columbia: basement of Quesnellia. In: Abstract and Program 15. Geological Association of Canada, p. A122.

Spear, F.S., 1993. Metamorphic Phase Equilibria and Pressure–Temperature–Time Paths. Mineralogical Society of America Monograph, Washington.

Spear, F.S., Cheney, J., 1989. A petrogenetic grid for pelitic schists in the system SiO_2–Al_2O_3–FeO–MgO–K_2O–H_2O. Contributions to Mineralogy and Petrology 101, 149–164.

Spear, F.S., Florence, F.P., 1992. Thermobarometry in granulites: pitfalls and new approaches. Precambrian Research 55, 209–241.

Spear, F.S., Parrish, R., 1996. Petrology and petrologic cooling rates of the Valhalla complex, British Columbia, Canada. Journal of Petrology 37, 733–765.

Tracy, R., Robinson, P., Thompson, A., 1976. Garnet composition and zoning in the determination of temperature and pressure of metamorphism, central Massachusetts. American Mineralogist 61, 762–775.

Varsek, J., Cook, F., 1994. Three-dimensional crustal structure of the eastern Cordillera, Southwestern Canada and Northwestern United States. Geological Society of America Bulletin 106, 803–823.

Vielzeuf, D., Clemens, J.D., 1992. The fluid-absent melting of phlogopite + quartz: experiments and models. American Mineralogist 77, 1206–1222.

Wheeler, J.O., Brookfield, A.J., Gabrielse, H., Monger, J.W.H., Tipper, H.W., Woodsworth, G.J. (Compilers), 1991. Terrane map of the Canadian Cordillera, Geological Survey of Canada Map 1713A, scale 1:2,000,000.

Williams, P.F., 1999. Interpretation of thrust-like structures in middle and lower crustal rocks. In: Tectonic and Magmatic Processes in Crustal Growth: a Pan-Lithoprobe Perspective. Lithoprobe Report 75, pp. 67–68.

Yardley, B., 1989. An Introduction to Metamorphic Petrology. Longman, London.